$Au_{38}(SPh)_{24}$: Au_{38} Protected with Aromatic Thiolate Ligands

Milan Rambukwella,[†] Shayna Burrage,[†] Marie Neubrander,[†] Oscar Baseggio,[‡] Edoardo Aprà,[§] Mauro Stener,[‡] Alessandro Fortunelli,[∥] and Amala Dass*,[†]

[†]Department of Chemistry and Biochemistry, University of Mississippi, Oxford, Mississippi 38677, United States
[‡]Dipartimento di Scienze Chimiche e Farmaceutiche, Università di Trieste, Trieste I-34127, Italy
[§]Pacific Northwest National Laboratory, Richland, Washington 99352, United States
[∥]CNR-ICCOM, Consiglio Nazionale delle Ricerche, Pisa, I-56124, Italy

Supporting Information

ABSTRACT: $Au_{38}(SR)_{24}$ is one of the most extensively investigated gold nanomolecules along with $Au_{25}(SR)_{18}$ and $Au_{144}(SR)_{60}$. However, so far it has only been prepared using aliphatic-like ligands, where $R = -SC_6H_{13}$, $-SC_{12}H_{25}$ and $-SCH_2CH_2Ph$. $Au_{38}(SCH_2CH_2Ph)_{24}$ when reacted with HSPh undergoes core-size conversion to $Au_{36}(SPh)_{24}$, and existing literature suggests that $Au_{38}(SPh)_{24}$ cannot be synthesized. Here, contrary to prevailing knowledge, we demonstrate that $Au_{38}(SPh)_{24}$ can be prepared if the ligand exchanged conditions are optimized, under delicate conditions, without any formation of $Au_{36}(SPh)_{24}$. Conclusive evidence is presented in the form of matrix-assisted laser desorption/ionization mass spectrometry (MALDI-MS), electrospray ionization mass spectra (ESI-MS) characterization, and optical spectra of $Au_{38}(SPh)_{24}$ in a solid glass form showing distinct differences from that of $Au_{38}(S\text{-aliphatic})_{24}$. Theoretical analysis confirms experimental assignment of the optical spectrum and shows that the stability of $Au_{38}(SPh)_{24}$ is not negligible with respect to that of its aliphatic analogous, and contains a significant component of ligand−ligand attractive interactions. Thus, while $Au_{38}(SPh)_{24}$ is stable at RT, it converts to $Au_{36}(SPh)_{24}$ either on prolonged etching (longer than 2 hours) at RT or when etched at 80 °C.

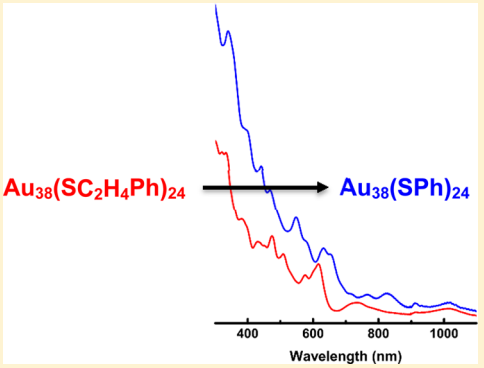

Gold nanomolecules[1,2] are ultrasmall gold nanoparticles <2 nm in size with a precise number of gold atoms protected by a specific number of thiolate ligands with distinct physical and chemical properties. They have become a topic of great interest in chemistry due to their atomic monodispersity (±0 atom variation), molecule-like properties,[3] and stability arising from geometric[4] and electronic shell[5] closings. These nanomolecules can be used in a wide variety of applications and can be made reproducibly and characterized by commonly available mass spectrometric, spectroscopic, and electrochemical methods.[3,6−13]

In previous work, we have published the first report of aromatic ligand induced core-size conversion of $Au_{67}(SR)_{35}$ and $Au_{103-105}(SR)_{44-46}$ nanocluster mixture to $Au_{36}(SPh)_{24}$, with its X-ray crystal structure reported subsequently.[14,15] This reaction was shown to proceed via a Au_{38} core as an intermediate in this reaction pathway. When the $-SCH_2CH_2Ph$ ligand was replaced by the −SPh ligand, the nanomolecule underwent an $Au_{38} \rightarrow Au_{36}$ core size conversion. This is believed to have been caused by the exchange of the aliphatic for the aromatic ligand, which being aromatic, bulkier, and rigid, would distort the Au_{38} structure. $Au_{38}(SR)_{24}$ core-size conversion to $Au_{36}(SR)_{24}$ has been reported, under harsh etching conditions (Scheme 1b). It was observed after an aromatic thiophenol ligand exchange of 10, that the Au_{38} intermediate converts to Au_{36} core.[14] Another subsequent report verified this conversion using Au_{38} as a starting material and studying ligand-induced core-size conversion of Au_{38} to Au_{36} in detail, in the presence of tertbutylbenzene thiophenol(TBBT) at elevated temperature (80 °C).[16] The reaction proceeds via a disproportionation mechanism with formation of a reaction intermediate, $Au_{40}(SR)_{26}$. We have reported the thiophenol-induced core-size conversion of $Au_{144}(SR)_{44}$ to $Au_{99}(SPh)_{42}$ and a $Au_{103-104}(SR)_{44-45}$ mixture to $Au_{102}(SPh)_{44}$, which shows evidence for the aromatic ligand-induced core-size conversion of a multiple species to one core-size, Au_{102} (refs 17 and 18). Also the aromatic ligand effect was evident by the core-size conversion of $Au_{144}(SR)_{60}$ to $Au_{133}(S\text{-PhtBu})_{52}$ with aromatic ligand *tert*-butylbenzenethiol(HS-PhtBu) (ref 19).

$Au_{38}(SR)_{24}$ readily forms when aliphatic-like ligands are used in direct synthesis[20,21] or etching,[22,23] whereas in the presence of aromatic ligands the Au_{38} core is found to be unstable, converting to Au_{36} (refs 14 and 16). Thus, existing literature suggests that all-aromatic $Au_{38}(SPh\text{-}X)_{24}$ nanomolecules cannot be synthesized.

Accepted: March 10, 2017

Scheme 1. $Au_{38}(SPh)_{24}$ Nanomolecules[a]

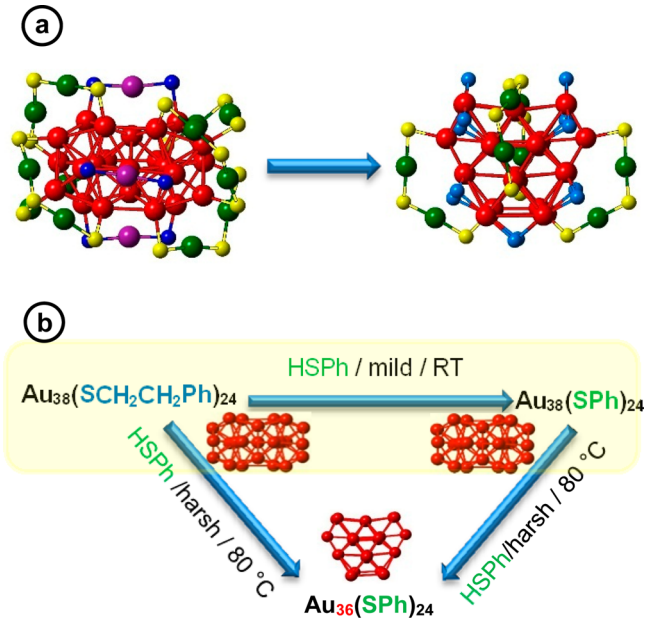

[a](a) Crystal structures of $Au_{38}(SCH_2CH_2Ph)_{24}$ and $Au_{36}(SPh)_{24}$ (red - core Au; green - dimeric staple Au; purple - monomeric staple Au; yellow-dimeric staple S; dark blue-monomeric staple S; light blue - bridging S). (b) $Au_{38}(SCH_2CH_2Ph)_{24}$ leading to form of either $Au_{38}(SPh)_{24}$ or $Au_{36}(SPh)_{24}$ based on reaction conditions.

Several questions, however, remain: Can we execute a systematic ligand exchange protocol to obtain all aromatic thiol protected $Au_{38}(SR)_{24}$ nanomolecules? What is the mechanism of the reaction, and would we observe a stable intermediate formation in the mechanism? How would extended conjugation with aromatic ligands modify electronic effects in the nanomolecule, and how significantly would it influence the band gap energy? How would aromaticity affect the overall electronic excitations?

To provide answers to these questions, here we study the ligand exchange and core-size conversion mechanism involved and the role of a particular ligand by executing a synthetic protocol on $Au_{38}(SR)_{24}$ nanomolecules, and we report the first synthesis of $Au_{38}(SPh)_{24}$ using a systematic two-step ligand exchange process on $Au_{38}(SCH_2CH_2Ph)_{24}$ under *mild* reaction conditions. The reaction method was executed to synthesize monodisperse all-aromatic ligand-protected $Au_{38}(SPh)_{24}$ species. Mass spectrometry and spectroscopic methods were utilized to verify the product. The product was then subject to low-temperature spectroscopic studies to obtain more insight into the electronic structure. These data are accompanied by a systematic theoretical study of the nanomolecule and its energetics, justifying the thermodynamic stability of aromatic $Au_{38}(SR)_{24}$ species and rationalizing the reasons for its greater sensitivity to environmental conditions.

In previous work, extensive theoretical and experimental studies have been reported on $Au_{38}(SR)_{24}$ and $Au_{36}(SR)_{24}$ nanomolecules. Single crystal X-ray diffraction studies have revealed their corresponding total structure (Scheme 1a,Table 1). $Au_{38}(SR)_{24}$ nanomolecules have a fused bi-icosahedral Au_{23} inner core protected with three $Au(SR)_2$ monomeric staples and six $Au_2(SR)_3$ dimeric staples.[24] By contrast, $Au_{36}(SR)_{24}$ nanomolecules possess a Au_{28} core with four interpenetrated cuboctahedrons, protected with four dimeric staples, and 12

Table 1. Comparison of $Au_{38}(SCH_2CH_2Ph)_{24}$ and $Au_{36}(SPh)_{24}$ Nanomolecules

Gold / Sulfur	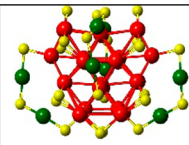	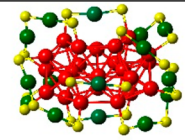
	$Au_{36}(SPh)_{24}$	$Au_{38}(SCH_2CH_2Ph)_{24}$
Symmetry	D_{2d}	D_3
Ligand Type	Aromatic	Aliphatic
Core	28	23
Geometry	Cuboctahedron	bi-icosahedron
Monomeric staples [SR-Au-SR]	0	3
Dimeric staples [SR-Au-SR-Au-SR]	4	6
Bridging thiols [SR]	12	0

bridging sulfurs that can also be viewed as another set of four dimeric staples (SPh-tBu[25], SPh[7]).

Thiophenol-protected $Au_{38}(SPh)_{24}$ nanomolecules were synthesized via ligand exchange on precursor $Au_{38}(SCH_2CH_2Ph)_{24}$ (Supporting Information Scheme S1). The precursor $Au_{38}(SCH_2CH_2Ph)_{24}$ nanomolecules was reacted with neat thiophenol ligand at room temperature (Scheme 2) in two stages: (1) In the first stage, a rapid ligand

Scheme 2. Synthetic Procedure for Monodisperse $Au_{38}(SPh)_{24}$[a]

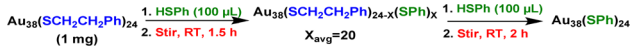

[a]In the first step, the reaction with HSPh yields partially exchanged $Au_{38}(SCH_2CH_2Ph)_{24-x}(SPh)_x$, where x_{avg} is 20. Successive second step yields completely exchanged $Au_{38}(SPh)_{24}$.

exchange with the $-SCH_2CH_2Ph$ was observed. Under these conditions, after 1.5 h, an average of 20 ligand exchanges can be achieved with no core-size conversion of $Au_{38}(SR)_{24}$ to $Au_{36}(SR)_{24}$. Note that, if the reaction is carried out for more than 1.5 h, it would result in core-size conversion of the starting material Au_{38} to $Au_{36}(SR)_{24}$. (2) In the second step, a second successive ligand exchange under identical conditions was carried out after purification of the product from first etch (Scheme 2, Figure 1). No $Au_{36}(SR)_{24}$ species was observed. An all-aromatic $Au_{38}(SPh)_{24}$ was observed after 2 h, as evidenced by mass spectrometry shown in Figure 2.

In Figure 2a, the electrospray ionization (ESI) mass spectrum of the product from step 2 upon addition of cesium acetate to facilitate ionization shows singly charged $[Au_{38}(SPh)_{24}{\cdot}Cs]^+$ and doubly charged, $[Au_{38}(SPh)_{24}{\cdot}2Cs]^{2+}$ species at 10 238 and 5186 m/z, respectively. The inset shows the comparison of the experimental and theoretical peaks for the 2+ species. The inset shows the theoretically calculated +1 peak against the experimental data. Figure 2b shows the matrix-assisted laser desorption/ionization (MALDI) mass spectra illustrating the molecular purity of the analyte, $Au_{38}(SPh)_{24}$. In the product, $Au_{36}(SPh)_{24}$ was not observed in this analysis, instead one ligand fragmented $Au_{38}(SPh)_{23}$ species was observed as noted before.[14] The inset illustrates the minor fragmentation at low laser due to labile nature of the thiophenol ligand.

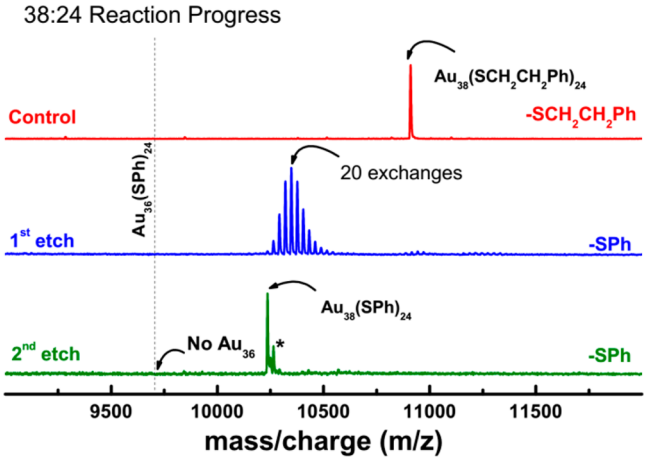

Figure 1. ESI mass spectra of the reaction between $Au_{38}(SCH_2CH_2Ph)_{24}$ and HSPh under optimized mild conditions to form $Au_{38}(SPh)_{24}$. First neat etching leads to $Au_{38}(SCH_2CH_2Ph)_{24-x}(SPh)_x$, a partial thiophenol ligand exchange, where x_{avg} = 20. Second etching gives the complete formation of $Au_{38}(SPh)_{24}$. All species are observed as Cs^+ adducts. No signal was observed for $Au_{36}(SPh)_{24}$. The peak marked by the asterisk depicts a trace amount of $Au_{38}(SPh)_{23}(SCH_2CH_2Ph)_1$.

MALDI-MS obtained at high laser fluence is a good indication of purity of nanomolecules. The characteristic fragmentation signature having $Au_4(SR)_4$ is prominently observed in small nanomolecules such as $Au_{25}(SR)_{18}$, $Au_{36}(SR)_{24}$, and $Au_{38}(SR)_{24}$ and can be used as an identification method of these nanomolecules, especially in a mixture, because the fragment peak is more prominent at higher laser fluence.[25−27] Figure 3a,b illustrates a detailed comparison of starting material $Au_{38}(SR)_{24}$ against a pure $Au_{36}(SR)_{24}$ "control" sample showing evidence of exclusive formation of $Au_{38}(SPh)_{24}$ and absence of $Au_{36}(SR)_{24}$ in the final product. Pure samples of $Au_{38}(SCH_2CH_2Ph)_{24}$, ligand-exchanged $Au_{38}(SPh)_{24}$, and $Au_{36}(SPh)_{24}$ nanomolecules were intentionally fragmented to observe the characteristic fragmentation (Figure 3a,b). In the final ligand-exchanged $Au_{38}(SPh)_{24}$ product, we did not observe $Au_{36}(SPh)_{23}$ or $Au_{32}(SPh)_{19}$ species, which indicates the absence of $Au_{36}(SPh)_{24}$. Also ultraviolet−visible−near-infrared (UV−vis−NIR) absorption profile of the product further illustrates the absence of well-defined optical features characteristic to $Au_{36}(SPh)_{24}$ and $Au_{38}(SCH_2CH_2Ph)_{24}$ nanomolecules (Figure 3c). Optical spectra of $Au_{38}(SPh)_{24}$ shows three distinct features from 425 to 725 nm: peaks at 470, 560, and 655 nm, whereas $Au_{38}(SCH_2CH_2Ph)_{24}$ shows two distinct absorption peaks at 445 and 620 nm. In contrast to the latter two nanomolecules, $Au_{36}(SPh)_{24}$ shows absorption features at 375 and 575 nm.

Temperature dependent UV−vis−NIR absorption spectra were measured in a solvent mixture of cyclohexane/cyclopentane 1:1 (v/v). Spectra shows increased intensities with a significant bathochromic shift in absorption maxima (red shift) at 78 K compared to room temperature, 298 K (Figure 4). Absorption intensity spectra plotted as the photon energy shows 11 well-resolved distinct peaks, and interestingly the peak at 1.7 eV was resolved into two new peaks. The temperature-dependent optical features of $Au_{38}(SCH_2CH_2Ph)_{24}$ shows that, upon reducing the temperature, the band gap increases.[28] By contrast, $Au_{38}(SPh)_{24}$ nanomolecules have an extended conjugation due to presence of the aromatic ring adjacent to the Au−S bridge. This results in a bathochromic shift, thereby reducing the band gap energy of the nanomolecule.

The structure and stability of $Au_{38}(SPh)_{24}$ were investigated theoretically. Starting from the experimentally determined crystal geometry of $Au_{38}(SCH_2CH_2Ph)_{24}$,[24] and after replacing the CH_2CH_2Ph with Ph residues, a local geometry optimization produced a geometry that was then used for property prediction and energy analysis (the full cluster Cartesian coordinates are reported in the Supporting Information). A relaxed geometry of $Au_{38}(SCH_2CH_2Ph)_{24}$ was also derived, as well as that of a $Au_{38}(SCH_3)_{24}$ cluster obtained from the relaxed geometry of $Au_{38}(SCH_2CH_2Ph)_{24}$ by replacing CH_2CH_2Ph

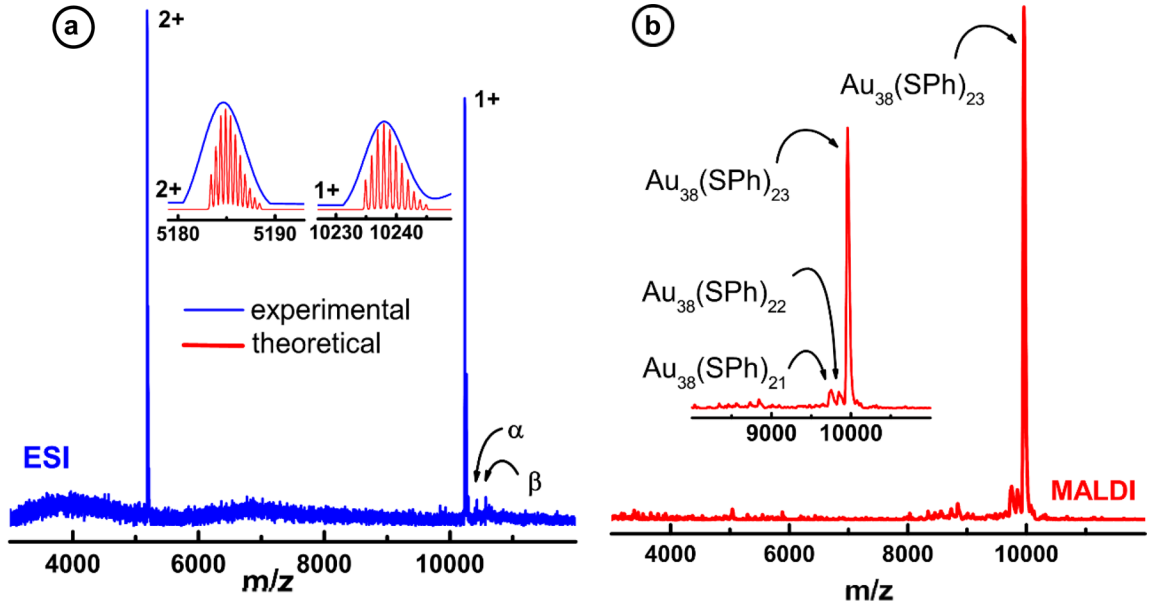

Figure 2. Evidence for the formation of $Au_{38}(SPh)_{24}$: (a) ESI mass spectra acquired with the addition of cesium acetate (blue), and inset shows the comparison of experimental and theoretical peaks for the 2+ species where peaks marked by α and β represent successive $CsCH_3COO$ addition on to the molecular peak. (b) MALDI mass spectra (red) and expansion of the fragmentation pattern.

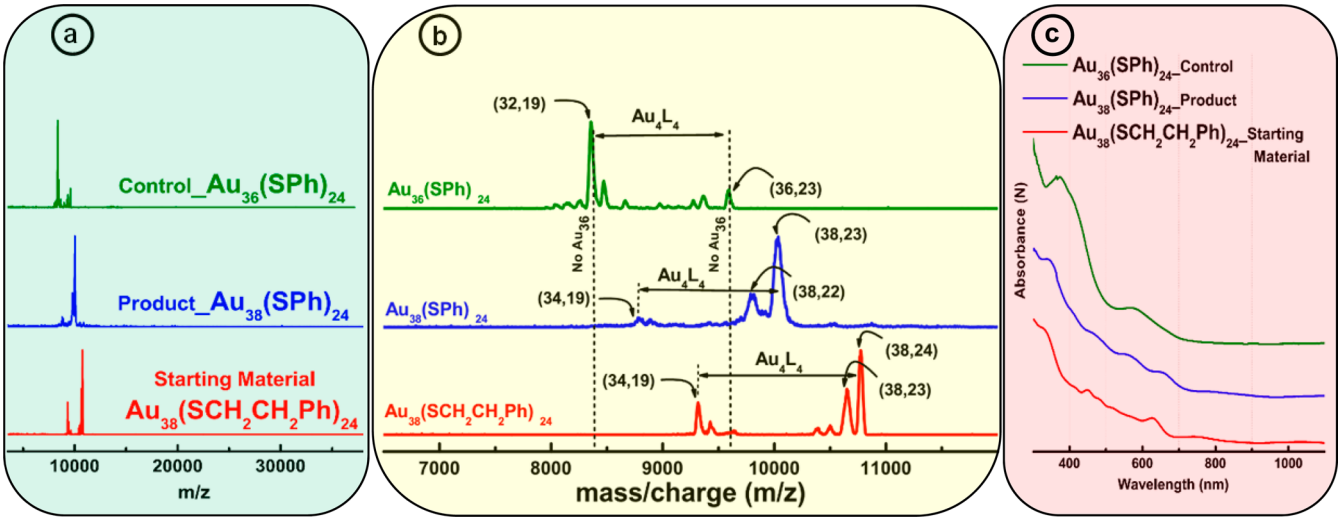

Figure 3. Evidence of the formation of $Au_{38}(SPh)_{24}$ and absence of $Au_{36}(SPh)_{24}$. (a) MALDI-TOF mass spectrum of the starting material, $Au_{38}(SCH_2CH_2Ph)_{24}$, and the final product, $Au_{38}(SPh)_{24}$, compared with a control sample, $Au_{36}(SPh)_{24}$. The data shows that only $Au_{38}(SPh)_{24}$ was synthesized. (b) MADLI-TOF mass spectrum showing the fragmentation patterns of three nanomolecules. (c) Comparison of UV–vis–NIR absorption spectrum features of $Au_{38}(SCH_2CH_2Ph)_{24}$, $Au_{38}(SPh)_{24}$, and $Au_{36}(SPh)_{24}$.

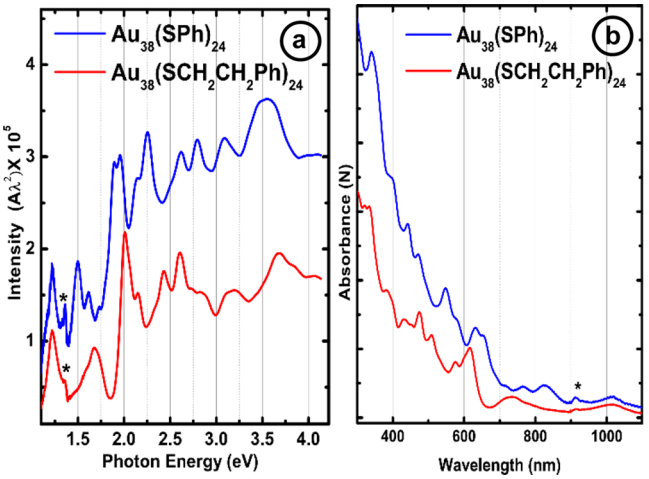

Figure 4. UV–vis–NIR optical spectrum of $Au_{38}(SPh)_{24}$ and $Au_{38}(SCH_2CH_2Ph)_{24}$ at 78 K: (a) energy plot; (b) absorption spectra. Peaks marked by an asterisk depict instrumental artifact.

with CH_3 residues and then optimizing their coordinates (keeping Au and S atoms frozen). Structure optimization does not bring about major changes in the $Au_{38}(SPh)_{24}$ cluster configuration, although some of the Au atoms in the −S−Au−S−Au−S− staples move slightly away from the Au core, as shown in Figure S6 of the Supporting Information. Here we assume that the replacement of aliphatic with aromatic ligands does not change the basic structure of the cluster, although we cannot exclude reconstructions [such as in Au_{28} (ref 29)].

An important question concerning $Au_{38}(SPh)_{24}$ is whether there are energetic factors, e.g., connected with electronic conjugation effects, that destabilize this gold nanomolecule with aromatic ligands. To assess the effects of electronic conjugation on energetics, we use energy decomposition and system comparison procedures proposed in previous work.[18,19,30−33] As a system to compare with, we use the aliphatic $Au_{38}(SCH_3)_{24}$ cluster derived from $Au_{38}(SCH_2CH_2Ph)_{24}$ as described above.

We first consider fragmentation reactions[33] for both the original and system-compared[19] clusters:

$$Au_{38}(SPh)_{24} \rightarrow Au_{38}[\text{fromPh}] + (SPh)_{24} \quad \Delta E = 82.5 \text{ eV} \tag{1}$$

$$Au_{38}(SCH_3)_{24} \rightarrow Au_{38}[\text{fromMet}] + (SCH_3)_{24} \quad \Delta E = 81.8 \text{ eV} \tag{2}$$

where the coordinates of the Au_{38} and $(SR)_{24}$ fragments on the right-hand-side of the equations are frozen in their interacting configurations. Fragmentation energies are sizable, but with only a minor ≈1% difference between them. This occurs despite the fact that the atomization energies of the metal fragments are quite different:

$$Au_{38}[\text{fromPh}] \rightarrow 38Au \quad \Delta E = 89.3 \text{ eV} \tag{3}$$

$$Au_{38}[\text{fromMet}] \rightarrow 38Au \quad \Delta E = 93.3 \text{ eV} \tag{4}$$

due to the detachment of Au atoms in the staples from the metal core in $Au_{38}(SPh)_{24}$ (Figure S6), which destabilizes the Au_{38} fragment. However, the loss of Au−Au binding is compensated by the strengthening of S−Au bonds,[30,32] finally resulting in an overall similar energy balance.

Next we consider the fragmentation of the crown or shell of ligands:[33]

$$(SPh)_{24} \rightarrow 24 \times SPh \quad \Delta E = 3.46 \text{ eV} \tag{5}$$

$$(SCH_3)_{24} \rightarrow 24 \times SCH_3 \quad \Delta E = 2.98\text{eV} \tag{6}$$

where the 24 SR thiols are still frozen internally but are separated at infinite distance in the processes of eqs 5 and 6. This fragmentation energy contains two terms: residual S−S binding (the sulfur atoms of thiols in the interacting configuration of the MPC are at binding distance) and dispersion/repulsion interactions between the organic residues. The latter contribution is negligible for $(SCH_3)_{24}$, but it can be substantial for $(SPh)_{24}$; we evaluate it by transforming the SPh ligands into HPh (i.e., thiols into benzene molecules) and calculating the fragmentation energy of the so-obtained benzene crown:[18,19]

$$(HPh)_{24} \rightarrow 24 \times HPh \quad \Delta E = 2.42 \text{ eV} \tag{7}$$

The sizable value of 2.42 eV for this process proves that part of the energetic stability of $Au_{38}(SPh)_{24}$, which makes it similar to its aliphatic $Au_{38}(SCH_3)_{24}$ analogue in terms of formation energy from eqs 1 and 2), is due to ligand−ligand attractive interactions such as $\pi-\pi$ and T-stackings among phenyl rings,[19] which overcome repulsive steric interactions (that are expected to be minor for this cluster as in $Au_{102}(SPh)_{44}$[18]). These stabilizing terms compensate for a decrease in residual S−S binding, associated with the weakening of S−S bonds due to conjugation effects—the counterpart of the noted strengthening of S−Au bonds.[30,32] It can be noted that the weakening of S−S bonds is not due to a variation of S−S distances, which indeed do not change much; the energy of a crown of thiomethyls obtained by transforming the phenyl residues of $(SPh)_{24}$ into methyls is similar to that of the analogue $(SCH_3)_{24}$ crown from $Au_{38}(SCH_3)_{24}$ (the energy difference is 0.54 eV in favor of the former).

In synthesis, ligand replacement,[18,30,32] between aliphatic and aromatic ligands, does not bring about qualitative changes in the system energetics. However, this results from a cancellation of contributions changing in the opposite sense. Notably, a significant component of the energetic stability of the aromatic $Au_{38}(SPh)_{24}$ is determined by ligand−ligand interactions, especially attractive dispersive interactions among the phenyl rings.[19] The fact that these interactions are expected to be sensitive to temperature and solvent effects is in keeping with the experimental observations summarized in Scheme 1. Note that our analysis is purely thermodynamic, and we do not investigate here possible contributions of kinetic effects to the cluster stability such as, e.g., found for $Au_{133}(SPh\text{-}tBu)_{52}$ due to dynamic fluctuation phenomena.[19]

Switching now to optical properties, Figure 5 reports a comparison between simulated and experimental photo-

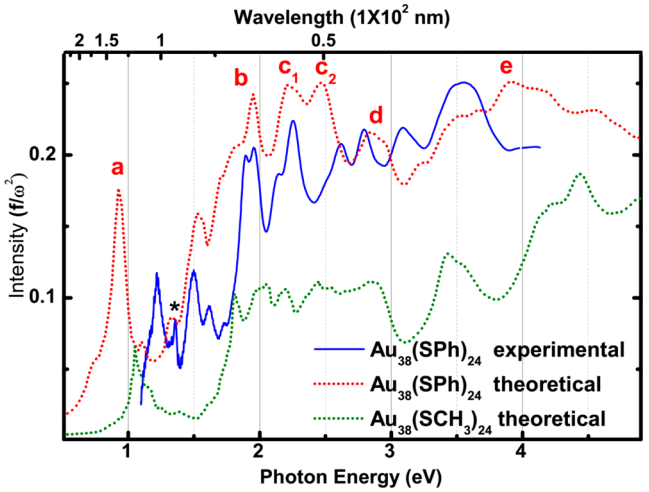

Figure 5. Comparison of experimental and simulated optical spectra of $Au_{38}(SPh)_{24}$ and simulated optical spectrum of $Au_{38}(SCH_3)_{24}$. Asterisk depicts an instrumental artifact.

absorption spectra of $Au_{38}(SPh)_{24}$. The fair agreement between simulated and measured spectra, including a bathochromic shift of the peaks with respect to the aliphatic counterpart, confirms the experimental assignment. Apart from this bathochromic shift, the overall similarity in appearance of the spectra may lead one to think that $Au_{38}(SPh)_{24}$ is not qualitatively different in terms of optical properties from its aliphatic analogues such as $Au_{38}(SCH_2CH_2Ph)_{24}$ (refs 28 and 34). However, a more punctual analysis produces a qualitatively different picture. As shown in Figure 6a, in fact, an analysis of the electronic excitations determining the optical spectrum of $Au_{38}(SCH_2CH_2Ph)_{24}$ in terms of atomic components[35] clearly shows that the transitions in the aliphatic compound are easily expressed as separate single-particle excitations, with the lowest-energy peak associated with HOMO−LUMO or HOMO−LUMO(+1) excitations. In $Au_{38}(SPh)_{24}$, instead, as partially shown in Figure 6b, electronic transitions are composed of many more single-particle excitations (see especially the c-peak at 2.40 eV) and with a strong presence of orbitals localized on the organic residues. Moreover, the lowest-energy transition is no longer associated with HOMO−LUMO or close excitations, but corresponds mostly to a HOMO(−4)−LUMO(+2) one. A major difference also concerns the intensity of the spectrum, a quantity less easily determined at the experimental level. Electronic conjugation in fact leads to an integrated intensity in the optical region roughly doubled in $Au_{38}(SPh)_{24}$ with respect to $Au_{38}(SCH_2CH_2Ph)_{24}$, despite the larger size (number of atoms) of the latter. In synthesis, in agreement with previous studies and proposals,[36−38] we find that electronic conjugation between organic residues and the (Au−S) system produces large effects in aromatic $Au_{38}(SPh)_{24}$. Attempts to synthesize $Au_{38}(SPhtBu)_{24}$ were unsuccessful and conversion to $Au_{36}(SPhtBu)_{24}$ occurs.

In conclusion, we present here the first synthesis and thorough experimental and theoretical characterization of a $Au_{38}(SR)_{24}$ nanomolecule containing purely aromatic ligands: R = Ph. Conclusive evidence of this achievement comes from MALDI-MS, ESI-MS characterization, and optical spectra of $Au_{38}(SPh)_{24}$ in a solid glass, and accompanying theoretical analysis. $Au_{38}(SPh)_{24}$ has a non-negligible interval of stability that is comparable to that of its aliphatic analogues, however, resulting from different physical origins, with a significant component connected with ligand−ligand attractive interactions, thus making it more sensitive to environmental conditions.

EXPERIMENTAL SECTION

Materials. Hydrogen tetrachloroaurate(III) ($HAuCl_4 \cdot 3H_2O$), sodium borohydride (Acros, 99%), thiophenol (Acros, 99%), phenyl-ethanemercaptan, (Sigma-Aldrich), cesium acetate (Acros, 99%), anhydrous ethyl alcohol (Acros, 99.5%), glutathione (Sigma-Aldrich, 98%), and trans-2-[3[(4-tertbutylphenyl)-2-methyl-2-propenylidene]malononitrile (DCTB matrix) (Fluka ≥99%) were used as received. HPLC-grade solvents such as tetrahydrofuran, toluene, methanol, butylated hydroxytoluene-stabilized tetrahydrofuran (THF), and acetonitrile were obtained from Fisher Scientific.

Synthesis. $Au_{38}(SCH_2CH_2Ph)_{24}$, was synthesized according to a previously reported procedure.[39] Complete aromatic ligand exchange on $Au_{38}(PET)_{24}$ nanomolecules to form $Au_{38}(SPh)_{24}$ without core-size conversion was performed in two main steps involving (i) a first ligand exchange with neat etching with excess thiophenol under mild conditions giving partially exchanged intermediate and (ii) a second neat etching to achieve complete ligand exchange to form $Au_{38}(SPh)_{24}$. First, $Au_{38}(SCH_2CH_2Ph)_{24}$ was reacted with excess thiophenol (HSPh, 100 μL/1 mg) at room temperature for 1.5 h. The product was then washed with methanol and subjected to a successive chemical treatment under the same conditions for 2

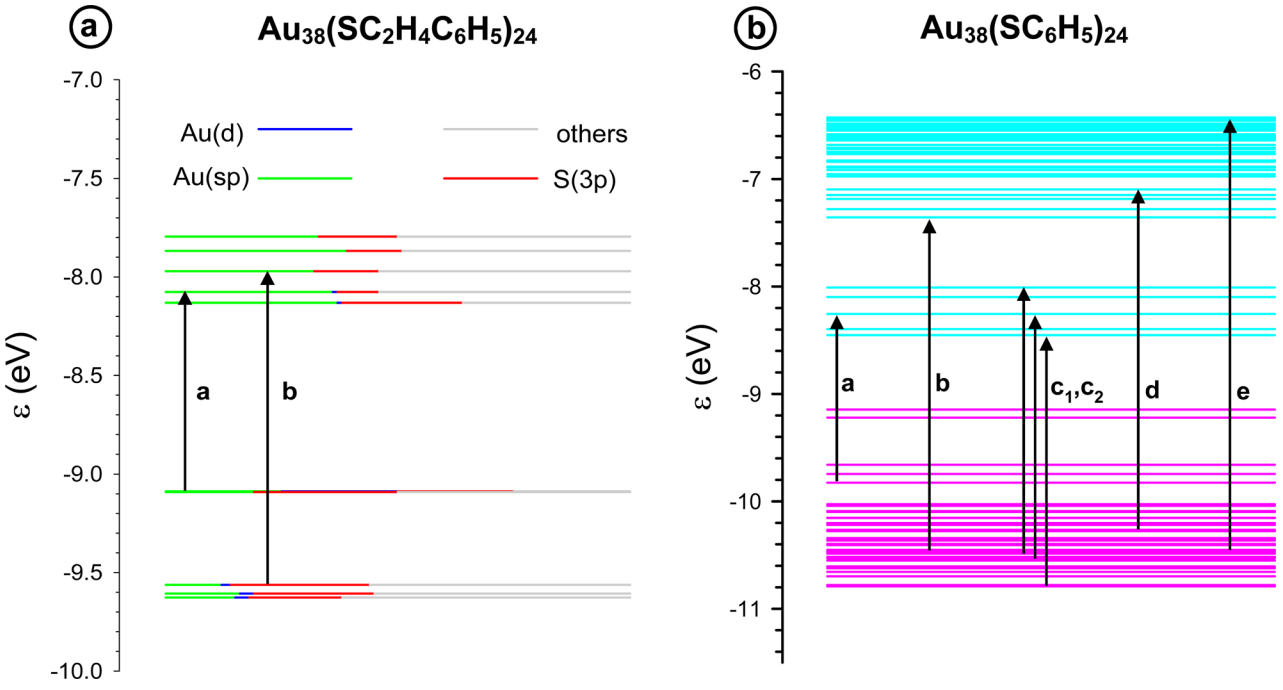

Figure 6. (a) Molecular orbital (MO) energies of $Au_{38}(SCH_2CH_2Ph)_{24}$ relevant for the analysis of its TDDFT photoabsorption spectrum. MOs are represented as horizontal lines colored in green, blue, red, and gray segments, whose length is proportional to the Mulliken contribution in the projection of the corresponding MO onto Au(6s6p), Au(3d), S(3s), and other atomic orbitals, respectively. Black arrows denoted by **a** and **b** visualize transitions relative to the spectral features at 0.95 and 1.75 eV respectively. (b) MO energies of $Au_{38}(SPh)_{24}$ relevant for the analysis of its TDDFT photoabsorption spectrum. MOs are represented as horizontal lines colored in pink and cyan for occupied and virtual orbitals, respectively. Black arrows denoted by **a**, **b**, **c1**, **c2**, **d**, and **e** visualize transitions relative to the spectral features at 0.95, 1.95, 2.22, 2.48, 2.85, and 3.95 eV, respectively.

h (see Scheme 2 and Figure 1). The final product was washed with methanol several times and extracted with toluene.

Instrumentation. A Voyager DE PRO mass spectrometer was used to acquire MALDI-TOF mass spectra using DCTB[40] matrix. Compositional analysis was performed with ESI-MS, collected from a Waters Synapt HDMS with THF as the solvent, and cesium acetate was added to facilitate ionization via cesium adduct formation of the analyte. Temperature-dependent UV−vis−NIR absorption data were measured with an UV−vis−NIR Cary 5000 and JANIS VNF-100 low-temperature cryostat using cyclohexane/cyclopentane 1:1 (v/v)as the solvent, and a Lakeshore Cyotronics temperature controller was used for temperature-dependent absorption measurements.

COMPUTATIONAL APPROACH

Geometry optimizations were performed using the Quantum Espresso code[41] and ultrasoft pseudopotentials.[42] A semi-empirical correction[43] was added to the Perdew−Burke−Ernzerhof (PBE)[44] exchange and correlation (xc-) functional to take into account the dispersion interaction between organic residues. The cutoff for the plane-wave representation of the wave function and the density were set to 40 and 400 Ry, respectively. In the local geometry optimizations, some of the atoms were kept frozen into configurations derived from X-ray measurements. In detail: in $Au_{38}(SPh)_{24}$ the Au_{23} core was taken from the $Au_{38}(SCH_2CH_2Ph)_{24}$ geometry reported in ref 24 (the rationale for this choice is that the PBE xc-functional describes reasonably well the Au−S, S−C, and C−H bonding, but is known to overestimate Au−Au distances). This experimental $Au_{38}(SCH_2CH_2Ph)_{24}$ geometry was also used to input the coordinates of all Au and S atoms in the relaxation of $Au_{38}(SCH_2CH_2Ph)_{24}$. From the relaxed geometry thus derived, a model $Au_{38}(SCH_3)_{24}$ system was obtained by replacing $-CH_2CH_2Ph$ with $-CH_3$ residues, and then relaxing only the atomic coordinates of the methyl groups.

Optical spectra were simulated at the time-dependent density functional theory (TDDFT) level, employing the recently developed complex polarizability algorithm,[45] implemented in a modified local version of the ADF code.[46] Such algorithm is more suited with respect to the conventional Casida scheme to calculate the spectrum for large systems to high energy, since does not suffer from the limitations connected with the Davidson diagonalization. The algorithm extracts the spectrum from the imaginary part of the complex dynamical polarizability, calculated point by point at the values of the light frequency. A Slater-Type Orbitals (STO) basis set of Triple Zeta plus Polarization (TZP) quality was employed. The asymptotically correct LB94 exchange-correlation potential[47] was employed for the resolution of the Kohn−Sham equations. The exchange-correlation kernel in the TDDFT equations was approximated by ALDA,[48] taking the derivative of the VWN LDA xc-potential.[49] The calculated spectra were smoothed by adding a small imaginary part (0.075 eV) to the real part of the frequency, corresponding to a Lorentzian broadening with the same half width at half maximum (HWHM). All the calculations were performed at scalar relativistic level with Zero Order Relativistic Approximation (ZORA).[50]

AUTHOR INFORMATION

Corresponding Author

*E-mail: amal@olemiss.edu.

ORCID

Edoardo Aprà: 0000-0001-5955-0734

Mauro Stener: 0000-0003-3700-7903

Alessandro Fortunelli: 0000-0001-5337-4450

Amala Dass: 0000-0001-6942-5451

Notes

The authors declare no competing financial interest.

ACKNOWLEDGMENTS

NSF 1255519, NSF 0903787, and NSF 1460568 supported the work performed by M.R., S.B., M.N., and A.D. Computational research was performed in part using EMSL, a DOE Office of Science User Facility sponsored by the Office of Biological and Environmental Research and located at Pacific Northwest National Laboratory, and PNNL Institutional Computing at Pacific Northwest National Laboratory. Support from CINECA supercomputing center within the ISCRA program is also gratefully acknowledged.

REFERENCES

(1) Tsukuda, T.; Hakkinen, H. *Protected Metal Clusters: From Fundamental to Applications*; Elsevier: Amsterdam, 2015.

(2) Whetten, R. L.; Khoury, J. T.; Alvarez, M. M.; Murthy, S.; Vezmar, I.; Wang, Z. L.; Stephens, P. W.; Cleveland, C. L.; Luedtke, W. D.; Landman, U. Nanocrystal Gold Molecules. *Adv. Mater.* **1996**, *8*, 428−433.

(3) Murray, R. W. Nanoelectrochemistry: Metal Nanoparticles, Nanoelectrodes, and Nanopores. *Chem. Rev.* **2008**, *108*, 2688−2720.

(4) Dass, A. Nano-scaling law: Geometric Foundation of Thiolated Gold Nanomolecules. *Nanoscale* **2012**, *4*, 2260−2263.

(5) Walter, M.; Akola, J.; Lopez-Acevedo, O.; Jadzinsky, P. D.; Calero, G.; Ackerson, C. J.; Whetten, R. L.; Gronbeck, H.; Hakkinen, H. A Unified View of Ligand-protected Gold Clusters as Superatom Complexes. *Proc. Natl. Acad. Sci. U. S. A.* **2008**, *105*, 9157−9162.

(6) Antonello, S.; Perera, N. V.; Ruzzi, M.; Gascón, J. A.; Maran, F. Interplay of Charge State, Lability, and Magnetism in the Molecule-Like $Au_{25}(SR)_{18}$ Cluster. *J. Am. Chem. Soc.* **2013**, *135*, 15585−15594.

(7) Pei, Y.; Zeng, X. C. Investigating the Structural Evolution of Thiolate Protected Gold Clusters from First-Principles. *Nanoscale* **2012**, *4*, 4054−4072.

(8) Aikens, C. M. Electronic Structure of Ligand-Passivated Gold and Silver Nanoclusters. *J. Phys. Chem. Lett.* **2011**, *2*, 99−104.

(9) Weissker, H. C.; Escobar, H. B.; Thanthirige, V. D.; Kwak, K.; Lee, D.; Ramakrishna, G.; Whetten, R. L.; López-Lozano, X. Information on Quantum States Pervades the Visible Spectrum of the Ubiquitous $Au_{144}(SR)_{60}$ Gold Nanocluster. *Nat. Commun.* **2014**, *5*, 3785.

(10) Knoppe, S.; Bürgi, T. Chirality in Thiolate-Protected Gold Clusters. *Acc. Chem. Res.* **2014**, *47*, 1318−1326.

(11) Jin, R. Atomically Precise Metal Nanoclusters: Stable Sizes and Optical Properties. *Nanoscale* **2015**, *7*, 1549−1565.

(12) Jadzinsky, P. D.; Calero, G.; Ackerson, C. J.; Bushnell, D. A.; Kornberg, R. D. Structure of a Thiol Monolayer-Protected Gold Nanoparticle at 1.1 Angstrom Resolution. *Science* **2007**, *318*, 430−433.

(13) Wong, O. A.; Heinecke, C. L.; Simone, A. R.; Whetten, R. L.; Ackerson, C. J. Ligand Symmetry-Equivalence on Thiolate Protected Gold Nanoclusters Determined by NMR Spectroscopy. *Nanoscale* **2012**, *4*, 4099−4102.

(14) Nimmala, P. R.; Dass, A. $Au_{36}(SPh)_{23}$ Nanomolecules. *J. Am. Chem. Soc.* **2011**, *133*, 9175−9177.

(15) Nimmala, P. R.; Knoppe, S.; Jupally, V. R.; Delcamp, J. H.; Aikens, C. M.; Dass, A. $Au_{36}(SPh)_{24}$ Nanomolecules: X-ray Crystal Structure, Optical Spectroscopy, Electrochemistry, and Theoretical Analysis. *J. Phys. Chem. B* **2014**, *118*, 14157−14167.

(16) Zeng, C.; Liu, C.; Pei, Y.; Jin, R. Thiol Ligand-Induced Transformation of $Au_{38}(SC_2H_4Ph)_{24}$ to $Au_{36}(SPh\text{-}t\text{-}Bu)_{24}$. *ACS Nano* **2013**, *7*, 6138−6145.

(17) Nimmala, P. R.; Dass, A. $Au_{99}(SPh)_{42}$ Nanomolecules: Aromatic Thiolate Ligand Induced Conversion of $Au_{144}(SCH_2CH_2Ph)_{60}$. *J. Am. Chem. Soc.* **2014**, *136*, 17016−17023.

(18) Rambukwella, M.; Sementa, L.; Barcaro, G.; Fortunelli, A.; Dass, A. Organosoluble $Au_{102}(SPh)_{44}$ Nanomolecules: Synthesis, Isolation, Compositional Assignment, Core Conversion, Optical Spectroscopy, Electrochemistry, and Theoretical Analysis. *J. Phys. Chem. C* **2015**, *119*, 25077−25084.

(19) Nimmala, P. R.; Theivendran, S.; Barcaro, G.; Sementa, L.; Kumara, C.; Jupally, V. R.; Apra, E.; Stener, M.; Fortunelli, A.; Dass, A. Transformation of $Au_{144}(SCH_2CH_2Ph)_{60}$ to $Au_{133}(SPh\text{-}tBu)_{52}$ Nanomolecules: Theoretical and Experimental Study. *J. Phys. Chem. Lett.* **2015**, *6*, 2134−2139.

(20) Chaki, N. K.; Negishi, Y.; Tsunoyama, H.; Shichibu, Y.; Tsukuda, T. Ubiquitous 8 and 29 kDa gold: Alkanethiolate Cluster Compounds: Mass-Spectrometric Determination of Molecular Formulas and Structural Implications. *J. Am. Chem. Soc.* **2008**, *130*, 8608−8610.

(21) Toikkanen, O.; Ruiz, V.; Ronnholm, G.; Kalkkinen, N.; Liljeroth, P.; Quinn, B. M. Synthesis and Stability of Monolayer-Protected Au_{38} Clusters. *J. Am. Chem. Soc.* **2008**, *130*, 11049−11055.

(22) Schaaff, T. G.; Whetten, R. L. Controlled Etching of Au: SR Cluster Compounds. *J. Phys. Chem. B* **1999**, *103*, 9394−9396.

(23) Nimmala, P. R.; Jupally, V. R.; Dass, A. Core Size Conversion: Route for Exclusive Synthesis of Au_{38} or Au_{40} Nanomolecules. *Langmuir* **2014**, *30*, 2490−2497.

(24) Qian, H.; Eckenhoff, W. T.; Zhu, Y.; Pintauer, T.; Jin, R. Total Structure Determination of Thiolate-Protected Au_{38} Nanoparticles. *J. Am. Chem. Soc.* **2010**, *132*, 8280−8281.

(25) Zeng, C.; Qian, H.; Li, T.; Li, G.; Rosi, N. L.; Yoon, B.; Barnett, R. N.; Whetten, R. L.; Landman, U.; Jin, R. Total Structure and Electronic Properties of the Gold Nanocrystal $Au_{36}(SR)_{24}$. *Angew. Chem., Int. Ed.* **2012**, *51*, 13114−13118.

(26) Angel, L. A.; Majors, L. T.; Dharmaratne, A. C.; Dass, A. Ion Mobility Mass Spectrometry of $Au_{25}(SCH_2CH_2Ph)_{18}$ Nanoclusters. *ACS Nano* **2010**, *4*, 4691−4700.

(27) Dass, A. Mass Spectrometric Identification of $Au_{68}(SR)_{34}$ Molecular Gold Nanoclusters with 34-Electron Shell Closing. *J. Am. Chem. Soc.* **2009**, *131*, 11666−11667.

(28) Devadas, M. S.; Bairu, S.; Qian, H.; Sinn, E.; Jin, R.; Ramakrishna, G. Temperature-Dependent Optical Absorption Properties of Monolayer-Protected Au_{25} and Au_{38} Clusters. *J. Phys. Chem. Lett.* **2011**, *2*, 2752−2758.

(29) Chen, Y.; Liu, C.; Tang, Q.; Zeng, C.; Higaki, T.; Das, A.; Jiang, D.-e.; Rosi, N. L.; Jin, R. Isomerism in $Au_{28}(SR)_{20}$ Nanocluster and Stable Structures. *J. Am. Chem. Soc.* **2016**, *138*, 1482−1485.

(30) Gao, Y.; Shao, N.; Zeng, X. C. Ab Initio Study of Thiolate-Protected Au_{102} Nanocluster. *ACS Nano* **2008**, *2*, 1497−1503.

(31) Reimers, J. R.; Wang, Y.; Cankurtaran, B. O.; Ford, M. J. Chemical Analysis of the Superatom Model for Sulfur-Stabilized Gold Nanoparticles. *J. Am. Chem. Soc.* **2010**, *132*, 8378−8384.

(32) Jung, J.; Kang, S.; Han, Y.-K. Ligand Effects on the Stability of Thiol-Stabilized Gold Nanoclusters: $Au_{25}(SR)_{18}^{-}$, $Au_{38}(SR)_{24}$, and $Au_{102}(SR)_{44}$. *Nanoscale* **2012**, *4*, 4206−4210.

(33) Crasto, D.; Barcaro, G.; Stener, M.; Sementa, L.; Fortunelli, A.; Dass, A. $Au_{24}(SAdm)_{16}$ Nanomolecules: X-ray Crystal Structure, Theoretical Analysis, Adaptability of Adamantane Ligands to Form $Au_{23}(SAdm)_{16}$ and $Au_{25}(SAdm)_{16}$, and Its Relation to $Au_{25}(SR)_{18}$. *J. Am. Chem. Soc.* **2014**, *136*, 14933−14940.

(34) Lopez-Acevedo, O.; Tsunoyama, H.; Tsukuda, T.; Häkkinen, H.; Aikens, C. M. Chirality and Electronic Structure of the Thiolate-Protected Au_{38} Nanocluster. *J. Am. Chem. Soc.* **2010**, *132*, 8210−8218.

(35) Zhu, M.; Aikens, C. M.; Hollander, F. J.; Schatz, G. C.; Jin, R. Correlating the Crystal Structure of A Thiol-Protected Au_{25} Cluster and Optical Properties. *J. Am. Chem. Soc.* **2008**, *130*, 5883−5885.
(36) Sementa, L.; Barcaro, G.; Dass, A.; Stener, M.; Fortunelli, A. Designing Ligand-Enhanced Optical Absorption of Thiolated Gold Nanoclusters. *Chem. Commun.* **2015**, *51*, 7935−7938.
(37) Dass, A.; Theivendran, S.; Nimmala, P. R.; Kumara, C.; Jupally, V. R.; Fortunelli, A.; Sementa, L.; Barcaro, G.; Zuo, X.; Noll, B. C. $Au_{133}(SPh\text{-}tBu)_{52}$ Nanomolecules: X-ray Crystallography, Optical, Electrochemical, and Theoretical Analysis. *J. Am. Chem. Soc.* **2015**, *137*, 4610−4613.
(38) Tlahuice-Flores, A.; Whetten, R. L.; Jose-Yacaman, M. Ligand Effects on the Structure and the Electronic Optical Properties of Anionic $Au_{25}(SR)_{18}$ Clusters. *J. Phys. Chem. C* **2013**, *117*, 20867−20875.
(39) Qian, H.; Zhu, Y.; Jin, R. Size-Focusing Synthesis, Optical and Electrochemical Properties of Monodisperse $Au_{38}(SC_2H_4Ph)_{24}$ Nanoclusters. *ACS Nano* **2009**, *3*, 3795−3803.
(40) Dass, A.; Stevenson, A.; Dubay, G. R.; Tracy, J. B.; Murray, R. W. Nanoparticle MALDI-TOF Mass Spectrometry without Fragmentation: $Au_{25}(SCH_2CH_2Ph)_{18}$ and Mixed Monolayer $Au_{25}(SCH_2CH_2Ph)_{18\text{-}x}(L)_x$. *J. Am. Chem. Soc.* **2008**, *130*, 5940−5946.
(41) Giannozzi, P.; Baroni, S.; Bonini, N.; Calandra, M.; Car, R.; Cavazzoni, C.; Ceresoli, D.; Chiarotti, G. L.; Cococcioni, M.; Dabo, I.; et al. QUANTUM ESPRESSO: A Modular and Open-Source Software Project for Quantum Simulations of Materials. *J. Phys.: Condens. Matter* **2009**, *21*, 395502.
(42) Vanderbilt, D. Soft Self-Consistent Pseudopotentials in a Generalized Eigenvalue Formalism. *Phys. Rev. B: Condens. Matter Mater. Phys.* **1990**, *41*, 7892−7895.
(43) Grimme, S.; Antony, J.; Ehrlich, S.; Krieg, H. A Consistent and Accurate Ab Initio Parametrization of Density Functional Dispersion Correction (DFT-D) for the 94 Elements H-Pu. *J. Chem. Phys.* **2010**, *132*, 154104.
(44) Perdew, J. P.; Burke, K.; Ernzerhof, M. Generalized Gradient Approximation Made Simple [Phys. Rev. Lett. 77, 3865 (1996)]. *Phys. Rev. Lett.* **1997**, *78*, 1396−1396.
(45) Baseggio, O.; Fronzoni, G.; Stener, M. A New Time Dependent Density Functional Algorithm for Large Systems and Plasmons in Metal Clusters. *J. Chem. Phys.* **2015**, *143*, 024106.
(46) Fonseca Guerra, C.; Snijders, G. J.; te Velde, G.; Baerends, J. E. Towards an Order-N DFT Method. *Theor. Chem. Acc.* **1998**, *99*, 391−403.
(47) van Leeuwen, R.; Baerends, E. J. Exchange-Correlation Potential with Correct Asymptotic Behavior. *Phys. Rev. A: At., Mol., Opt. Phys.* **1994**, *49*, 2421−2431.
(48) Gross, E. K. U.; Kohn, W. Time-Dependent Density-Functional Theory. In *Advances in Quantum Chemistry*; Per-Olov, L., Ed.; Academic Press: Cambridge, MA, 1990; Vol. 21, pp 255−291.
(49) Vosko, S. H.; Wilk, L.; Nusair, M. Accurate Spin-Dependent Electron Liquid Correlation Energies for Local Spin Density Calculations: a Critical Analysis. *Can. J. Phys.* **1980**, *58*, 1200−1211.
(50) van Lenthe, E.; Baerends, E. J.; Snijders, J. G. Relativistic Regular Two-Component Hamiltonians. *J. Chem. Phys.* **1993**, *99*, 4597−4610.